Tip-sample characterization in the AFM study of a rod-shaped nanostructure

Tip-sample characterization in the AFM study of a rod-shaped nanostructure

To cite this article before publication: Gian Bartolo Picotto *et al* 2020 *Meas. Sci. Technol.* in press https://doi.org/10.1088/1361-6501/ab7bc2

Tip-sample characterization in the AFM study of a rod-shaped nanostructure

Gian Bartolo Picotto (1), Marta Vallino (2), Luigi Ribotta (1,3)*

(1) Istituto Nazionale di Ricerca Metrologica (INRiM), Strada delle Cacce 91, 10135, Torino, Italy
(2) Consiglio Nazionale delle Ricerche – Istituto per la Protezione Sostenibile delle Piante (CNR – IPSP), Strada delle Cacce 73, 10135, Torino, Italy
(3) Politecnico di Torino, Corso Duca degli Abruzzi 24, 10129, Torino, Italy

*corresponding author: l.ribotta@inrim.it

Abstract

Accurate measurements of linewidth standards, sidewalls and non-spherical nanoparticles performed at the nanoscale by means of Atomic Force Microscopy suffer from errors due to the tip shape and size. In order to reduce the uncertainty, the study here presented aims at investigating a bio-plant nanostructure, namely the Tobacco Mosaic Virus, as candidate reference tip characterizer.

The TMV has a rod-shaped structure with a diameter of about 18 nm early reported from X-ray fibre diffraction, thus representing a reference at the nanoscale. When imaged by the AFM, the diameter of the TMV is determined as the top height of the rod from the reconstructed cross-section profile of isolated virions, deposited on a flat substrate like mica. A mean diameter of 16.5 nm, smaller than the nominal value by fibre diffraction measurements, is determined with our metrological AFM. Meanwhile, tip-sample-substrate interactions are discussed with reference to experimental data and models in literature, in order to determine deformations and associated uncertainty of corrections, with which the difference between the AFM-reconstructed top-height diameter and the nominal value reduces to about 0.3 nm.

Once the virus is fully characterised, a tip profile is estimated by the AFM-reconstructed cross-section profiles of the TMV. The approach used is to evaluate the tip-related enlargement from the nominal circle size, assumed undeformed, of the TMV cross-section profile. A good repeatability of the reconstructed tip shape is achieved from subsequent imaging of virions, while tip degradations are somewhat visible over the working time.

Keywords: Atomic Force Microscopy, Tobacco Mosaic Virus (TMV), tip characterizer, tip-sample interactions

1. Introduction

The development of nanotechnologies and the progressive miniaturisation in top-down and bottom-up processes in chemistry, physics and biology require new reference materials, which must be able to guarantee the accuracy of measurements methods and instrumentations used in nanoscience and nanotechnology. Traceable 3D measurements of nanoparticles (NPs) are today an issue, where both size and shape of structures play a crucial role at the nanoscale. Many of the functional properties of

nanoparticulate materials depend on their particle size, which can be accurately measured for mono-disperse nanoparticles with spherical shape, as demonstrated in interlaboratory comparisons [1,2], while it is somewhat a challenge for particles of complex geometry.

In dimensional measurements, the traceability chain starts from the national meter sample, and arrive at the nanoscale through stabilized laser sources and interferometers coupled to microscopes. Among these, metrological Atomic Force Microscopes (mAFMs), usually developed in the NMIs, make use of interferometric systems to measure the tip-sample relative position. Anyhow, also these high-resolution microscopes need further calibration and characterisation to reduce measurements uncertainty. The AFM technique allows measuring the out of plane dimension of nano-objects with sub-nanometer accuracy. The in-plane lateral resolution, however, is affected by the tip finite size, and without a calibration of the tip geometry and the study of tip-sample interactions, significant errors in the measurements of complex geometry nanostructures and line-width samples can be done. The convolution effect became more significant when tip dimensions are comparable to the sample critical dimensions. Moreover, the convolution is due to the adhesion forces between the sample and the substrate, and to the force applied to the tip. In AFM-based step-height measurements of flat steps, the impact of the tip geometry is negligible and the tip-sample interactions at the top/bottom planes are self-compensating; instead, 3D imaging/profiling is a bi-directional measurement process, where the effect of tip geometry broadens the feature of interest and tip-sample interactions at the left and right sidewalls and top of structures are different. The interactions between the AFM tip and the sample have been deeply investigated, starting from the Hertzian model of elastic deformations [3] to models of elastic/elastoplastic deformations [4,5,6], that introduced surface forces. These models are now widely used to investigate tip-sample interactions either with inorganic [7] and biological [8] samples.

For AFM tip characterizers, sharply pointed features are commercially available, but these characterizers lack on traceability and can lead to damaging standard AFM silicon tips when performing several measurements, as demonstrated by Slattery [9] while measuring niobium and titanium calibration samples. Besides, more expensive line-width standards are also available, but less common for a frequent daily use.

The dimensional characteristics of the tip can be extracted from external analyses of the probe (e.g. electron/optical microscopy), but the main drawback is that those characteristics are assessed under different experimental conditions, like temperature, state of the AFM tip, scan speed, force between tip and sample etc. [10]. Moreover, optical or electron microscopic methods do not directly provide 3D information, require removal and reinsertion of the tip, and suffer from their own probe-sample convolution effects [11]. For these reasons, a method that allows to determine the morphology of the tip *in situ*, without moving it from the microscope support, would be useful. Furthermore, the tip, given its small size, can change its morphology and be modified in performing several measurements. The development of reference nanomaterials [12] will lower uncertainties in the lateral resolution of images and improve the traceable calibration of measuring instruments. Over the years, several studies about tip characterisation have been presented, including (i) AFM measurements of physical artefacts [13,14,15] (*e.g.* spheres [16] and conical structures [17]) and (ii) *in situ* blind reconstruction techniques from unknown sample geometry [18,19,20]. It must be remembered that the use of physical artefacts as tip characterizer permits highly accurate and traceable dimensional measurements [21].

AFM is a versatile scanning probe technique, and the ability of imaging soft samples without damaging in different environmental media (air and liquid) makes this microscope technique a powerful tool for the study of biological samples. Therefore, natural nanostructures such as Tobacco Mosaic Virus (TMV), are candidate to be used as reference material for AFM tip reconstruction geometry and tip-sample interaction analysis. The peculiarity of using TMV as reference materials is that its geometry is particularly suitable for performing AFM top-height measurements [22,23,24]. Moreover, being a nanostructure from nature, TMV does not require synthesis equipments, and it is worldwide available. Furthermore, the advantage of using

TMV as tip characterisation standard is that the virus has a low elastic modulus and a simple cylindrical geometry with a stable top-height diameter when imaged in the same operating conditions in non-contact mode, so there are not hard sharp and steep edges that can bring to tip fractures, as it happens when scanning sharp structures with high moduli [9].

In the following, TMV sample preparation are presented in section 2, quantitative AFM top-height measurements of the TMV are reported in section 3, while in section 4 the tip reconstruction is studied.

2. Materials and Methods

2.1 The Tobacco Mosaic Virus

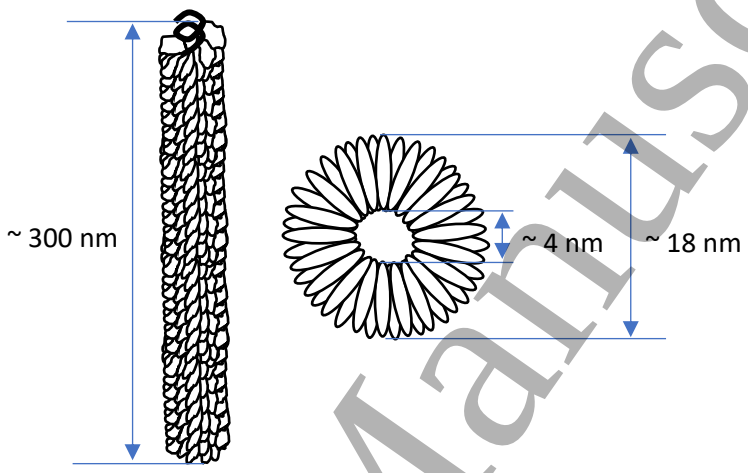

Figure 1 TMV structure sketch.

Tobacco Mosaic Viruses are part of the Tobamoviruses family, and are characterized by a rod-shape structure (Figure 1), as reported in [25], for a total length of about 300 nm, with an inner diameter of 4 nm and outer diameter of 18 nm; these values come from fibre diffraction studies [26,27,28,29]. In sample preparation this virus can break, and so they can vary their length, but the diameter size do not undergo alterations, and so can be used as reference dimension for tip calibration, since the virus looks stable in air conditions [30] once deposited on mica substrate. In our experience, in few cases it is possible that small fragment of virus contaminated the tip, as reported in [22] for non-contact measurements.

2.2 Sample preparation

Several *Nicotiana benthamiana* plants are mechanically inoculated with Tobacco Mosaic Virus (TMV) strain "T9" stored in CNR – IPSP (Consiglio Nazionale delle Ricerche – Istituto per la Protezione Sostenibile delle Piante) Plant Virus Italy (PLAVIT) Collection as "dried leaf" [31].

An aliquot of dried leaves is taken from the collection and crushed with mortar and pestle in 50 mM phosphate buffer, pH 7.0, containing 1 mM Na EDTA, 5 mM Na DIECA and 5 mM Na thioglycolate, added with activated charcoal. The homogenate is used for mechanical inoculation on *N. benthamiana* leaves previously dusted with carborundum powder as an abrasive.

After viral symptoms appeared (about one week), symptomatic leaves are collected and stored at -80 °C. 20 g of leaves are used for TMV particles purification. Leaves are crushed in liquid nitrogen using mortar and pestle and then homogenized in 80 ml (1:4 w:v) of extraction buffer (0.25 M potassium phosphate

buffer, pH 7.0, 0.5 % thioglycolic acid, and 10 mM EDTA). The homogenate is filtered through a gauze, mixed with an equal volume of chloroform and stirred for 15 min at 4 °C. After centrifugation at 10 000 rpm for 10 min at 4 °C, the supernatant is layered onto a 10 ml 20 % sucrose cushion prepared in the extraction buffer and centrifuged for 60 min at 40 000 rpm at 4 °C. The resulting pellet is dissolved in 2 ml of the extraction buffer and centrifuged for 1 min at 16 000 rpm. The supernatant is layered on a 10 to 50 % sucrose gradient in extraction buffer and centrifuged for 2 h at 36 000 rpm. A large band is collected and centrifuged at 100 000 rpm for 1 h. The pellet is dissolved in 0.05 M K-phosphate buffer, pH 7.0 and centrifuged for 1 min at 16 000 rpm. The supernatant is recovered and stored a -20 °C. To check for purity and for viral particles integrity and quantity, the extract is observed under an electron microscope. A drop of the purification is allowed to adsorb for 1 min on carbon and formvar-coated grids and then rinsed several times with water. Grids are negatively stained with 0.5 % uranyl acetate and excess fluid is removed with filter paper. Serial dilutions of the purification are prepared in water and observed, in order to reach a concentration in which viral particles are abundant but well separated and not overlapping. The instrumentations used for a qualitative analysis of the TMV batches is the CM 10 Philips TEM with fluorescence detector, using an electronic beam energy of 60 kV, and the FEI Inspect F SEM in modality STEM, using an electronic beam energy of 20 kV (Figure 2).

A drop of 20 ml of the chosen dilution, prepared in MilliQ water, is then deposited on freshly cleaved mica and let to air dry (Figure 3).

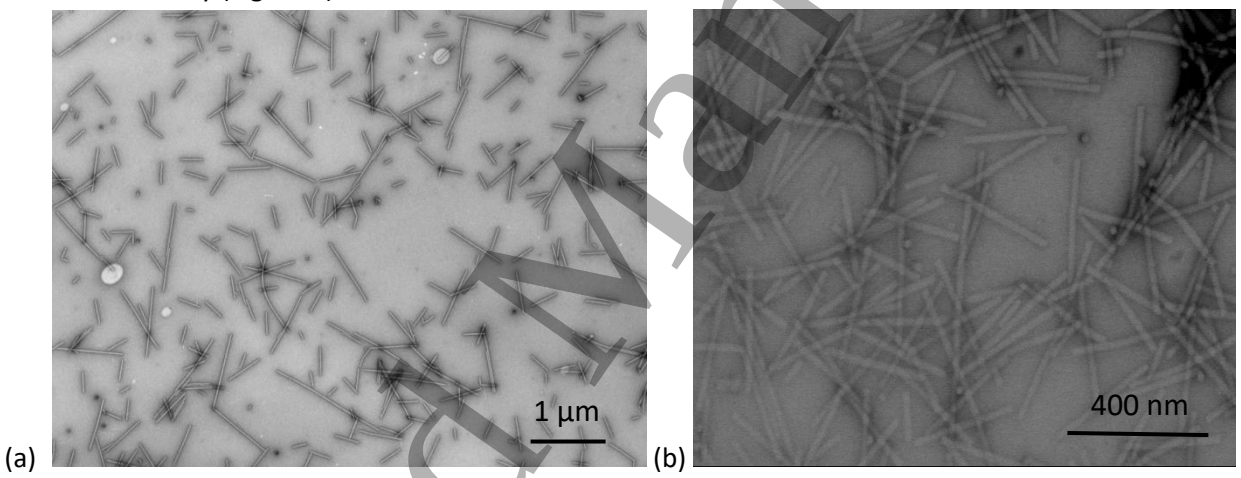

Figure 2 (a) TEM and (b) STEM micrographies of TMV. Images respectively from CNR-IPSP and INRiM Nanofacility Piemonte.

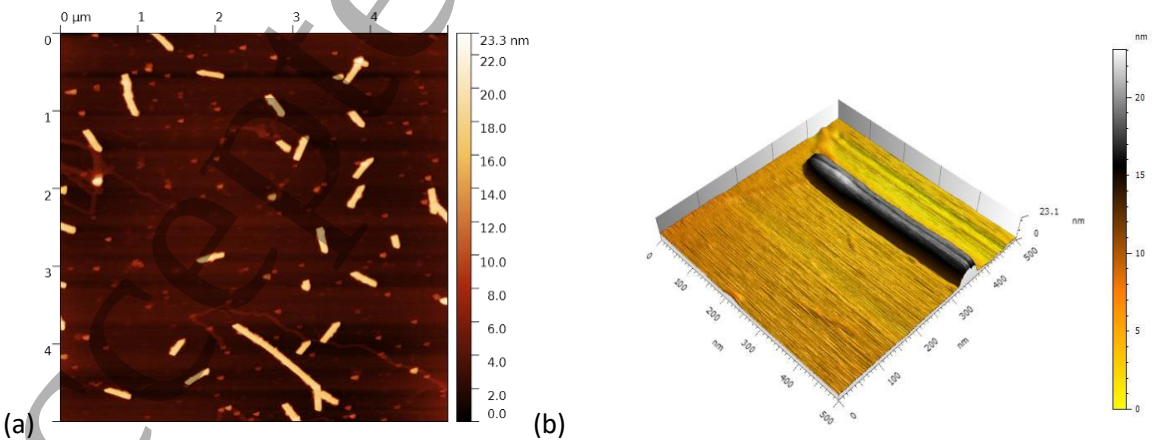

Figure 3 (a) AFM top-view image of the TMVs from a diluted batch deposited on mica; virions are somewhat broken or attached to each other and appearing longer. In figure (b) a 3D view of a single virion.

3. AFM analysis on TMV samples

The AFM imaging is a combination of the sample shape, the tip-sample-substrate interactions and the tip geometry [32]. In this work all these three contributions are considered, and in particular the TMV critical dimensions and the tip-TMV interactions are described in section 3. It must be bare in mind that AFM images show an apparent broadening of lateral dimensions due to the finite tip size, and the 2D tip geometry reconstruction is reported in section 4.

3.1 TMV diameter and lateral characterization

Once the TMV batch is diluted without the presence of organic residues, the samples are quantitatively analyzed with the INRiM metrological AFM [33]. Measurements are performed in laboratory with controlled humidity at (20.0 ± 0.1) °C, according to the ISO 1 [34]. The AFM measurement modality used is non-contact measurement with amplitude modulation. Measurements are performed using commercial n-type silicon tips by µMasch [35], with a nominal radius of 8 nm, a nominal resonance frequency of 325 kHz (frequency range 265 Hz – 410 Hz) and a nominal force constant of 50 Nm $^{-1}$ (force constant range 20 Nm $^{-1}$ – 80 Nm $^{-1}$).

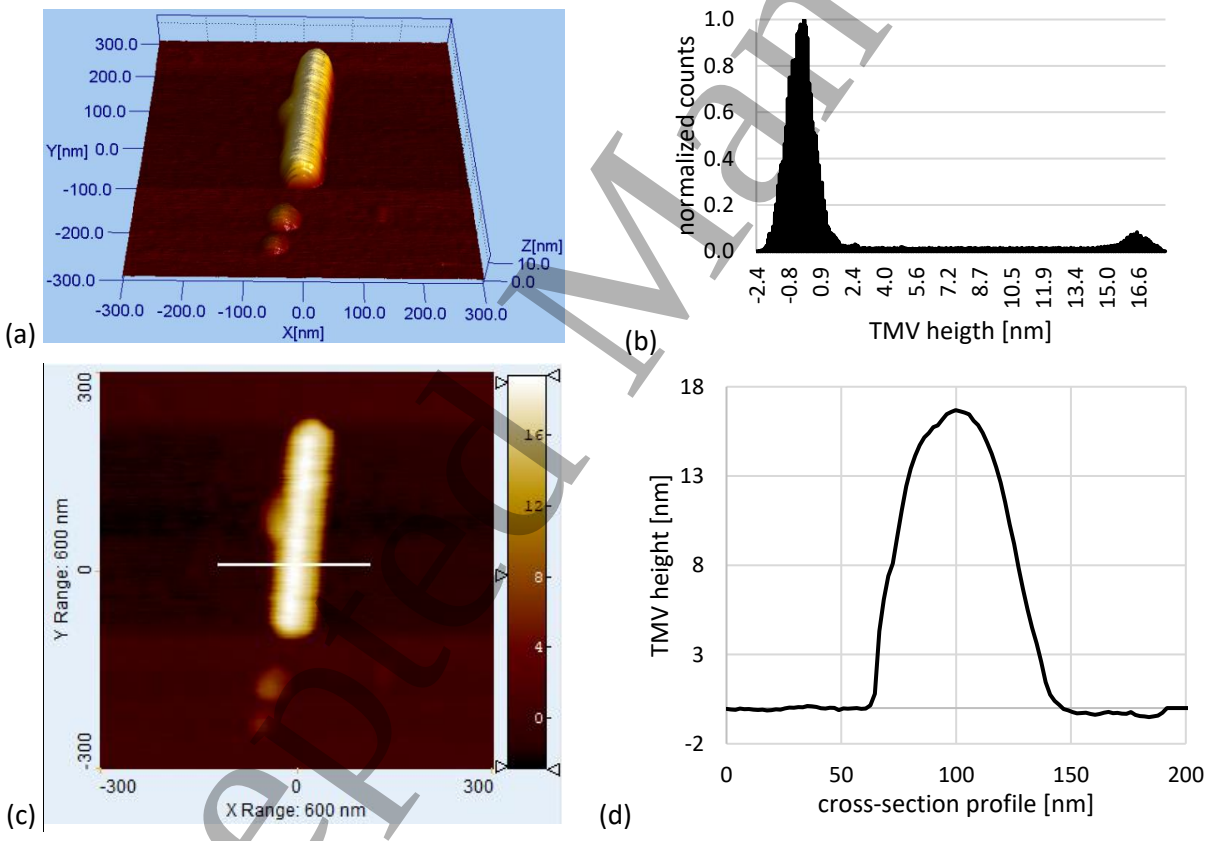

Figure 4 (a) 3D mAFM micrograph of an isolated TMV, (b) its normalized height histogram, and (c, d) its cross-section profile.

Several mAFM images from (300 × 300) nm to (500 × 500) nm with resolution (512 × 512) pixels centred on isolated TMV nanostructures are processed thanks to the tools of the software SPIP [36].
The first characterisation concerns the TMV diameter determination as thickness of the TMV cross-section profile, as reported in Figure 4 (c) and (d). Moreover, the same measurand is determined by the height histogram tool, in which the highest peak refers to the height of the substrate pixels and is centred at 0 nm,

while the smallest peak is referred to the virus top. Note that these two independent measurements of the diameter resulted well in agreement within 1 %.

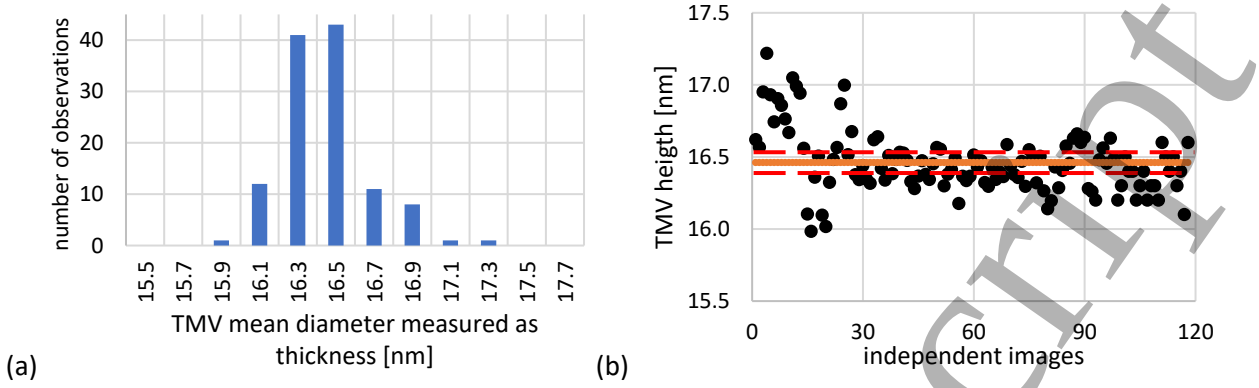

Figure 5 TMV diameters measured as thickness of the virus cross-section profile from 120 mAFM images. (a) Histogram and (b) experimental values reported together with the average value (orange line). The red sparse dotted lines refer to standard deviation of the mean.

Figure 5 reports the TMV diameters measured as the top-height, or otherwise called thickness, of the cross-section profiles from 120 independent images recorded using 6 different tips on 3 different samples deposited on freshly cleaved mica. It can be appreciated that this measure looks almost stable, robust and repeatable, while the outliers due to noisy images are not considered in our study. Image processing is a very delicate operation, inasmuch the use of filters may significantly alter topological dimensions, thus substantially changing the measurand. For this reason, in order not to alter the critical dimensions of the virus with respect to the substrate, the images are subjected to the rotation of the inclined plane, naturally present in each SPM image, due to the misalignment between the substrate plane and the tip scan plane, and to the image levelling by SPIP tools. TMV diameters reported in Figure 5 (a) and (b) are obtained as average of the thicknesses measured at the right and the left of the virus mean cross-section profile by means of cursors, one placed at the virus top and the other on the mica substrate. For these measurements the step-height tool (ISO 5436) is not used, since this latter leads to TMV thicknesses that are about 1 nm smaller compared to the measurements performed with cursors. In fact, ISO 5436 tool is designed for step-height measurements between flat steps and is not suitable for rounded profiles, such as that of TMV cross-section profile.

As reported in Figure 5 (b) the average TMV diameter value is 16.5 nm, which is smaller than the nominal value by X-ray fibre diffraction measurements of 18 nm. This result underline the well-known issue of the comparability of the same measurand by different techniques, also reported in the international comparison on nanoparticle size APMP-L.S5 [2].

Please note that the nominal value of 18 nm is extensively used in literature to describe TMV diameter [26,27,28,29], but according to the different methods used to determine the measurand from X-ray measurements, values of 18.6 nm (minimum zone diameter) [30], 16 nm (hard core diameter), 18 nm (minimum diameter) and 19 nm (maximum diameter) [37] can also be find.

Moreover, it is worth noting that TMV diameter values smaller than the nominal value are also reported in literature from AFM-based measurements on isolated viruses, with values are strongly dependent to the imaging environment and the substrate; TMV top-height of about 16.5 nm in air on mica [30,38,39], 14 nm on hydrophilic (O_2-plasma treated) silicon substrates [40] and about 18.2 nm in liquid on mica [37,41] are registered. We assume that the reason why AFM top-height diameter is smaller than the nominal value is the interaction between the tip, the sample and the substrate, as discussed in section 3.3.1. It is worth noting that a mean diameter of about 17.8 nm is reported from AFM measurements of packed TMV viruses

(mean lateral size) [30], which may suffer from TMV-TMV lateral deformation; one may justify the difference between nominal diameter to that from lateral packed virions by using the Hertzian contact theory, as discussed in the reference [3].

In order to fully characterize the virions, also lateral dimensions are analysed. Note that measurements are performed on the X-profiles taken along the fast scanning axis, in order to (i) detect the asymmetric profile due to the tip geometry and (ii) avoid the effect of drifts and noise due to uncompensated mechanical drifts, that can be appreciated tracing a profile along the Y-axis of the image. Note that these lateral measurements are useful to characterize the apex tip size and geometry, described in paragraph 4.

Figure 6 (a) reports the average TMV cross-section profiles taken from virions on 3 samples subsequently prepared and imaged along a period of more than one year. A total of 6 different tips were used with these samples, each tip taking about 30 images. The data reported are average values for each tip that derive from the analysis of the mean cross-section profiles of the viruses to determine the width of the profile at different heights, namely at the bottom (~ 0 nm), and at heights of about 8 nm, 12 nm, 14 nm, 15 nm and 16.5 nm from the mica substrate. Figure 6 (b) shows the trend of a TMV cross-section profile through the average points, obtained from the analysis of several profiles from different images registered with a single tip. Figure 6 (c) shows the entity of the profile asymmetry due to the tip geometry, since profile is centred respect to the maximum height; as a term of comparison, a symmetric profile is also shown in this plot, considering the absolute value of each lateral enlargement at the various heights.

Figure 6 (d) shows the incremental trend of the lateral dimensions due to tip dilation, because the continued use lead to the tip wear.

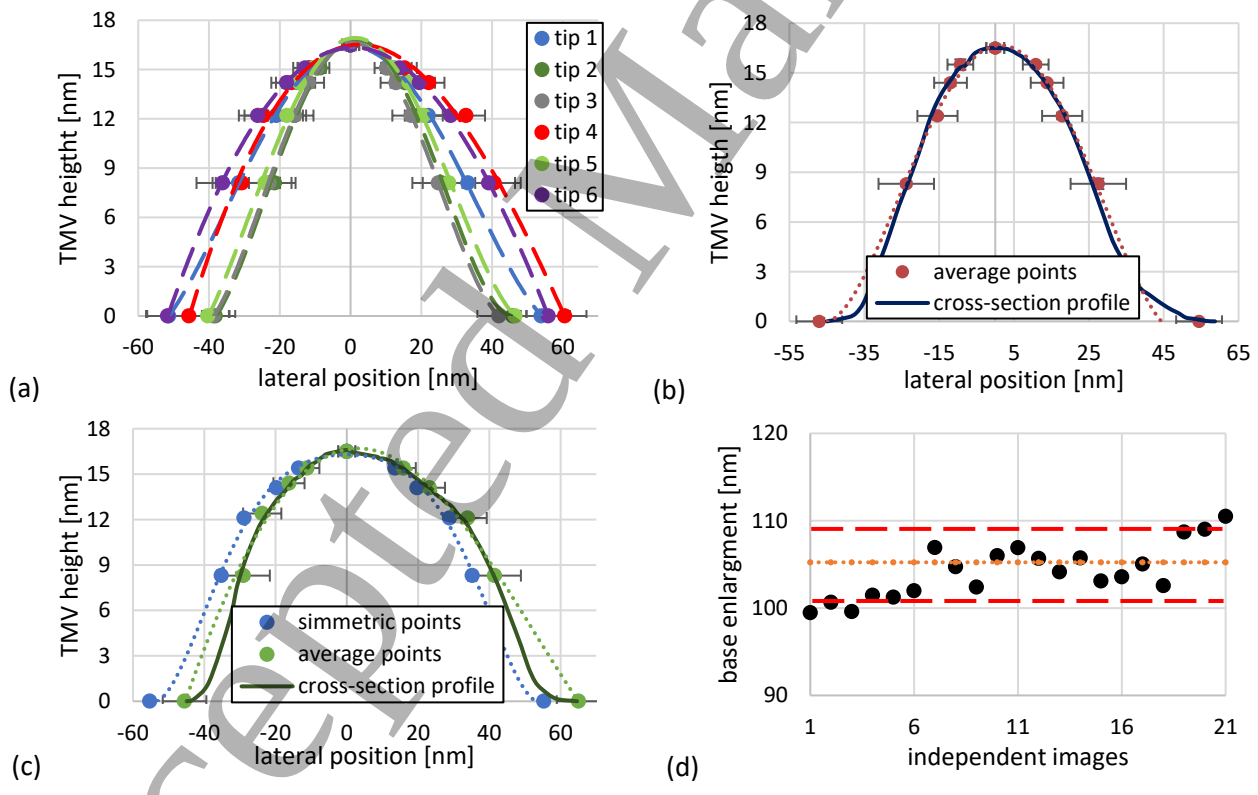

Figure 6 (a) Reconstruction of TMV cross-section mean profiles from the lateral measurement of images measured by different tips. (b) Comparison between a cross section profile and average points from several images registered with the same tip. (c) Comparison between a symmetric-made cross-section profile and a true asymmetric profile due to the tip geometry. The error bars in (a), (b) and (c) refer to measurements' standard deviation. (d) Increment in lateral dimensions due to the tip wear; in orange Is reported the average enlargement, while the red sparse dotted lines in refer to standard deviation of the mean.

3.2 Experimental estimation of the TMV elastic modulus

In order to estimate the modulus of elasticity of a nanostructure, such as the TMV, the elastic cantilever constant is determined, so that the spring constant converts the cantilever deflection into a calibrated force, essential for measuring the Young modulus [42]. To do that, the behaviour changes of the tip from a rest position up to the interaction with the sample is firstly checked. Data on the variation of the tip amplitude oscillation *vs*. applied Z piezoelectric offset are reported in Figure 7. The Z piezoelectric offset is manually applied in steps of 0.5 V from -10 V to +10 V, and since the maximum stroke of the piezoelectric used is about 2 µm, a conversion factor $c_{offset} = 98\ \mathrm{nm/V}$ is determined. Also the amplitude oscillation is registered in volts, so for calculating the conversion factor $c_{amplitude} = 217\ \mathrm{nm/V}$, the pitch of the screw that adjust the laser beam on the photodiode is measured, and the factor calculated is corrected for the amplification due to the optical lever of the laser beam on the photodiode.

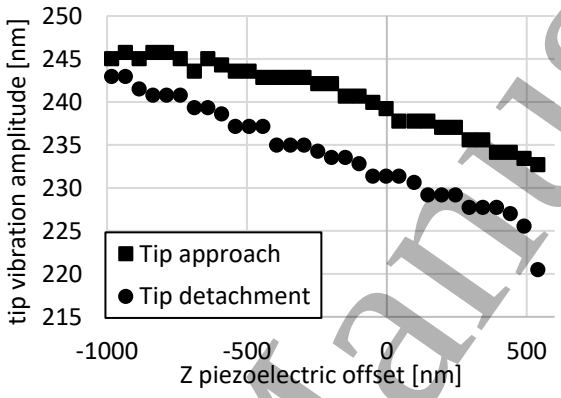

Figure 7 Variation of the tip amplitude oscillation vs. applied Z piezoelectric offset

Various methodologies to determine the elastic cantilever constant have been developed, that can be divided in (i) theoretical methods, such as Euler Beam equation and Cleveland formula [43], Sader resonance method [44], and Sader hydrodynamic method [45], (ii) static methods, in which a trial cantilever is pressed against a reference one [46,47], and (iii) dynamic methods, which require knowledge of the cantilever resonance behaviour [48,49]. In order to calibrate the cantilever used to perform our measurements, we use the Global Calibration Initiative tool [50,51], that combine Sader and thermal methods giving a constant of 47.8 N·m^{-1} with a 10 % relative standard uncertainty. This tool permits the calibration of cantilever without damaging it, directly comparing the calibration results with the worldwide AFM community users.

Among others, several experimental values of the TMV Young modulus by AFM indentation tests are reported in literature. Falvo *et al.* [52] report a value of about $1.1\ \mathrm{GPa}$, obtained through the manipulation with the AFM silicon nitrite tip (*i.e.* rotations and bendings) of TMV viruses deposited onto a graphite substrate. Kiselyova *et al.* [53] estimate a Young modulus of about $3\ \mathrm{GPa}$ based on measurements of indentation on TMV deposited on mica substrate. Schmatulla *et al.* [54] study the TMV Young modulus by means of a silicon nitrite tip using two methods: (i) static method ($\mathrm{E} = (6.8 \pm 2.4)\ \mathrm{GPa}$), in which the TMV is deposited onto a polycarbonate substrate and it is trapped in a solvent bubble, and (ii) dynamic method ($\mathrm{E} = (5.0 \pm 3.8)\ \mathrm{GPa}$), in which the TMV lays at one end on the mica substrate and at the other end on another virus. Zhao *et al.* [55] perform indentation measurements on viruses deposited onto mica, by means of a silicon nitride tip with a radius of about 15 nm in an open liquid cell in contact mode. By using the Hertz model he obtains a Young modulus of $\mathrm{E} = (1.0 \pm 0.2)\ \mathrm{GPa}$, while from finite element analysis $\mathrm{E} = (0.92 \pm 0.15)\ \mathrm{GPa}$. Wang *et al.* [56] perform indentation measurements by using a silicon tip with a radius of 12 nm on 2D hexagonal packed rod-like superlattice structure assembled from TMVs, obtaining an elastic modulus

of $\mathrm{E} \sim 2.14\ \mathrm{GPa}$ through the application of Johnson–Kendall–Roberts (JKR) model to experimental data, while using finite element analysis the Young modulus is calculated in the range $(2.00 - 4.38)\ \mathrm{GPa}$, depending on indentation locations.

The reduced modulus E_{red} is calculated using the Hertzian model reported in Equation (1) [57], where $k = 47.8\ \mathrm{N{\cdot}m^{-1}}$ is the elastic cantilever constant calibrated as explained above, $\nu_{TMV} = 0.48$ is the TMV Poisson's ratio [55] and A is the tip-sample interaction area.

$$E_{red} = \frac{1}{2} \cdot k \cdot (1 - \nu_{TMV}^2) \cdot \sqrt{\frac{\pi}{A}} \qquad (1)$$

The TMV Young modulus E_{TMV} is calculated according to the Equation (2), that is the inversed formula of the reduced modulus [57]; $E_{tip} = 170\ \mathrm{GPa}$ [58] and $\nu_{tip} = 0.24$ [59] are respectively the Young modulus and the Poisson's ratio of the silicon tip.

$$E_{TMV} = \frac{E_{red} \cdot E_{tip} \cdot (1 - \nu_{TMV}^2)}{E_{tip} - E_{red} \cdot (1 - \nu_{tip}^2)} \qquad (2)$$

Tip radius of about $(12 - 15)\ \mathrm{nm}$ have been estimated in some reports cited above for the calculation of the Young modulus. Through the analysis of the top of cross-section profiles of TMV from AFM images, we estimate a tip radius of $20\ \mathrm{nm}$, with which $E_{TMV} = 0.7\ \mathrm{GPa}$ is calculated. Meanwhile, by assuming the nominal tip radius of 8 nm, a Young modulus $E_{TMV} = 1.8\ \mathrm{GPa}$ is obtained. Therefore, the mean value $E_{TMV} = 1.3\ \mathrm{GPa}$ is obtained, considering $8\ \mathrm{nm}$ and $20\ \mathrm{nm}$ as the limit of a rectangular distribution of the radius of the tip-sample interaction area. Since the Young modulus value is strongly influenced by the interaction area, an expanded uncertainty of $0.6\ \mathrm{GPa}$ is estimated by means of the error propagation law: the main contribution comes from the reduced Young modulus, due to the uncertainty from the tip radius; minor contributions are due to the elastic cantilever constant and to the tip and TMV Poisson ratios, these last three assumed with a 10 % relative standard uncertainty.

3.3 Evaluation of tip-sample-substrate interactions

3.3.1 Tip-sample and tip-substrate elastic deformations

Elastic compression concerning the tip-sample and tip-substrate interactions are analysed considering the Hertzian model of contact mechanics [3]. This is therefore a first approximation for the tip-sample deformation, as the measurements are made in non-contact mode. To calculate the tip-TMV elastic deformation, the interaction of a sphere (representing the tip apex) with a cylinder (representing the TMV) is considered. The interaction between the tip and the mica substrate is analysed considering the contact between a sphere (representing the tip apex) and a plane (representing the mica substrate).

3.3.2 Sample-substrate adhesion deformation

Johnson–Kendall–Roberts (JKR) [4], Derjaguin–Muller–Toporov (DMT) [5] and Maugis–Pollock (MP) [6,60,61] models describe the elastic/plastic deformation between a sphere and a plane. The contact radius s between the sphere and the plane is described by JKR as $s = \sqrt[3]{\frac{6 \cdot \pi \cdot w_a \cdot {r_{TMV}}^2}{K}}$, by DMT as $s =$

$\sqrt[3]{\frac{2\cdot\pi\cdot w_a\cdot {r_{TMV}}^2}{K}}$ and by MP as $s=\sqrt{\frac{2\cdot w_a\cdot r_{TMV}}{3\cdot Y}}$. In order to describe the elastoplastic sample-substrate deformation due to the interaction between the TMV rod and the flat mica substrate, we make use of the approach by Chaudhury *et al.* [62], thus calculating the interaction between a cylinder and a plane with a lateral half side contact of $c=\sqrt[3]{\frac{128\cdot w_a\cdot {r_{TMV}}^2}{3\cdot\pi\cdot K}}$. Note that the equivalent elastic modulus is $K=\frac{4}{3}\cdot\left[\frac{1-\nu_{TMV}^2}{E_{TMV}}+\frac{1-\nu_{mica}^2}{E_{mica}}\right]^{-1}$, with the evaluated $E_{TMV}=1.2$ GPa, $\nu_{TMV}=0.48$ [55], $E_{mica}=190$ GPa and $\nu_{mica}=0.25$ [63], and the TMV yield point is $Y=20$ MPa [64]. w_a is the work caused by an adhesion between the particle and the substrate and it is given by $w_a=2\sqrt{\gamma_{part}\cdot\gamma_{sub}}$, where γ_{part} is the TMV surface energy is considered to be $\gamma_{part}=50$ mJ/m^2, from the estimation of the surface tension of amino acids that are present on the virus surface [64], and $\gamma_{sub}=48$ mJ/m^2 [2] is the mica surface energy in air.

All the sample-substrate deformations reported in Table 1 are calculated according to the following formula $\alpha=r_{TMV}-\sqrt{{r_{TMV}}^2-s^2}$ or $\alpha=r_{TMV}-\sqrt{{r_{TMV}}^2-c^2}$. Note that for our case study the model of interest is the cylinder on flat, but as a comparison also the deformation values calculated using the sphere on flat models are given as well, resulting that the cylinder-plane deformation is slightly minor that the average value from sphere-plane deformation models.

Table 1 Interaction between AFM tip-TMV, TMV-mica substrate, AFM tip-mica substrate.

	model	**parameter name**	$\Delta\alpha$ **[nm]**
tip-sample	Hertz (sphere-cylinder)	$\alpha_{tip-sam}$	0.40
sample-substrate	MP (sphere-plane)	$\alpha_{sam-sub\ MP}$	1.81
	JKR (sphere-plane)	$\alpha_{sam-sub\ JKR}$	0.99
	DMT (sphere-plane)	$\alpha_{sam-sub\ DMT}$	0.46
	Chaudhury *et al.* (cylinder-plane)	$\alpha_{sam-sub\ Ch}$	0.79
tip-substrate	Hertz (sphere-plane)	$\alpha_{tip-sub}$	0.02

The calculated deformations are summarized in Table 1, and it should be noted that the parameters Y, w_a and E_{TMV} have an important influence on the calculated deformation [65].
Since the TMV diameter measured as thickness give us a mean value of 16.5 nm, considering the tip-sample and the sample-substrate deformations, as calculated respectively by the Hertz and Chaudhury *et al.* approaches, we obtain a corrected TMV diameter of 17.7 nm. The tip-substrate deformation has a negligible effect, that can be considered in the image noise.

3.4 Uncertainty budget on TMV step-height profile measurements

Table 2 Uncertainty budget for the TMV diameter measured as TMV thickness. Note that N refers to a normal probability distribution function, while R refers to a rectangular probability distribution function.

uncertainty sources	***probability distribution***	***degrees of freedom*** v_i	***uncertainty*** $u_c(h)$ **[nm]**
repeatability	N	120	0.10
AFM calibration	N	50	0.25
profile noise	N	50	0.20
uncompensated mechanical drifts	R	50	0.20
tip geometry	R	10	0.30
correction of tip-sample interaction	R	20	0.10
correction of sample-substrate deformation	R	10	0.25
combined standard uncertainty		**82**	**0.60**

Table 2 reports the uncertainty budget for the TMV diameter measured as thickness. The main contributions are the z-interferometric calibration, including Abbe offset, optical non-linearity, dead-path and cosine errors, and the tip geometry considers the apex finite size. Another significant contribution is the uncertainty of the sample-substrate deformation, estimated assuming a rectangular probability distribution of size the largest calculated deformation by using Chaudhury *et al.* approach, while minor contributions are due to (i) the repeatability on measurements performed by the metrological set-up, (ii) tip-sample elastic interaction, profile noise, evaluated from the rms roughness of the substrate only, and (iii) uncompensated mechanical drifts, evaluated from the total height of the roughness profile R_t of the substrate only.

4. TMV as AFM tip characterizer

The tip shape characterisation is needed for a wide variety of applications, including dimensional measurements, nano-mechanics, chemical force and some electrical and magnetic modes [42]. As an example, to characterize the effective tip width at the highest accuracy, critical dimensions of line width on a standard photomask have been performed by PTB and NIST using CD-AFM instruments [66]. In this work, we chose to use TMV virus for characterising commercial AFM tips, because (i) it has a cylindrical geometry simple to characterize, a (ii) it has a stable measurand, that is the diameter, which size is in the range of the nominal radius of the AFM tip apex, and (iii) it is a nanostructure almost worldwide available from nature.

An initial unsuccessful approach that we use to characterize the geometry of the tips, is the tip characterisation software tool, which uses the "blind reconstruction" method [13]; this method would require a sample more rough than the flat mica to get more insights into the tip size.

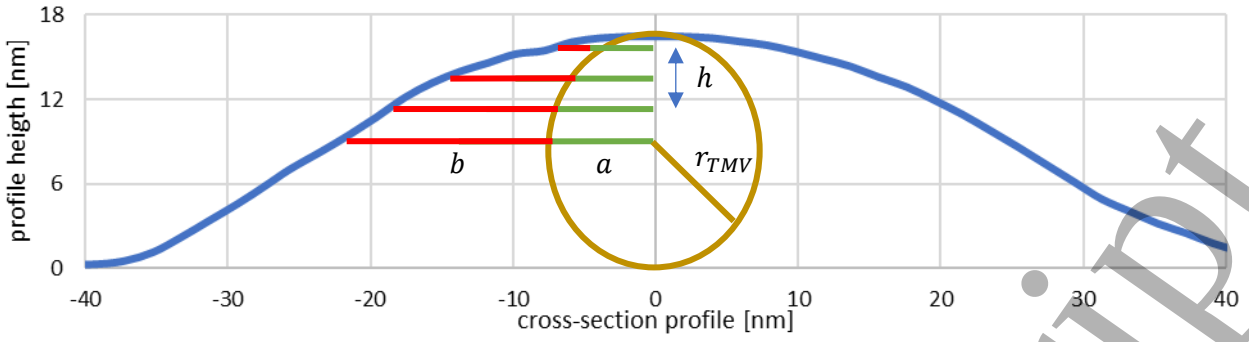

Figure 8 In-scale sketch reporting the experimental cross-section profile (in blue), give from the convolution of the cross-section TMV (in yellow) and the tip. Note that a is the chord of the circle and b is the enlargement.

In order to estimate the 2D cross-section profile of the tip along the X fast scanning axis of the image data [21], the TMV sample is used as "tip" for characterizing the silicon tip, that is now our "unknown sample". Figure 8 show how the experimental cross-section profile is influenced by the tip geometry; by assuming the known circle shape and size of the TMV virion, we can quantify the tip-related enlargement, i.e., a and b, and subsequently estimate the tip geometry. Note that $a = \sqrt{h\,(2r_{TMV} - h)}$ is the semi-chord of the circle, while b is the right/left profile enlargement due to the tip, and h is the difference between the top circle height to the height of the chord at which is calculated the enlargement.

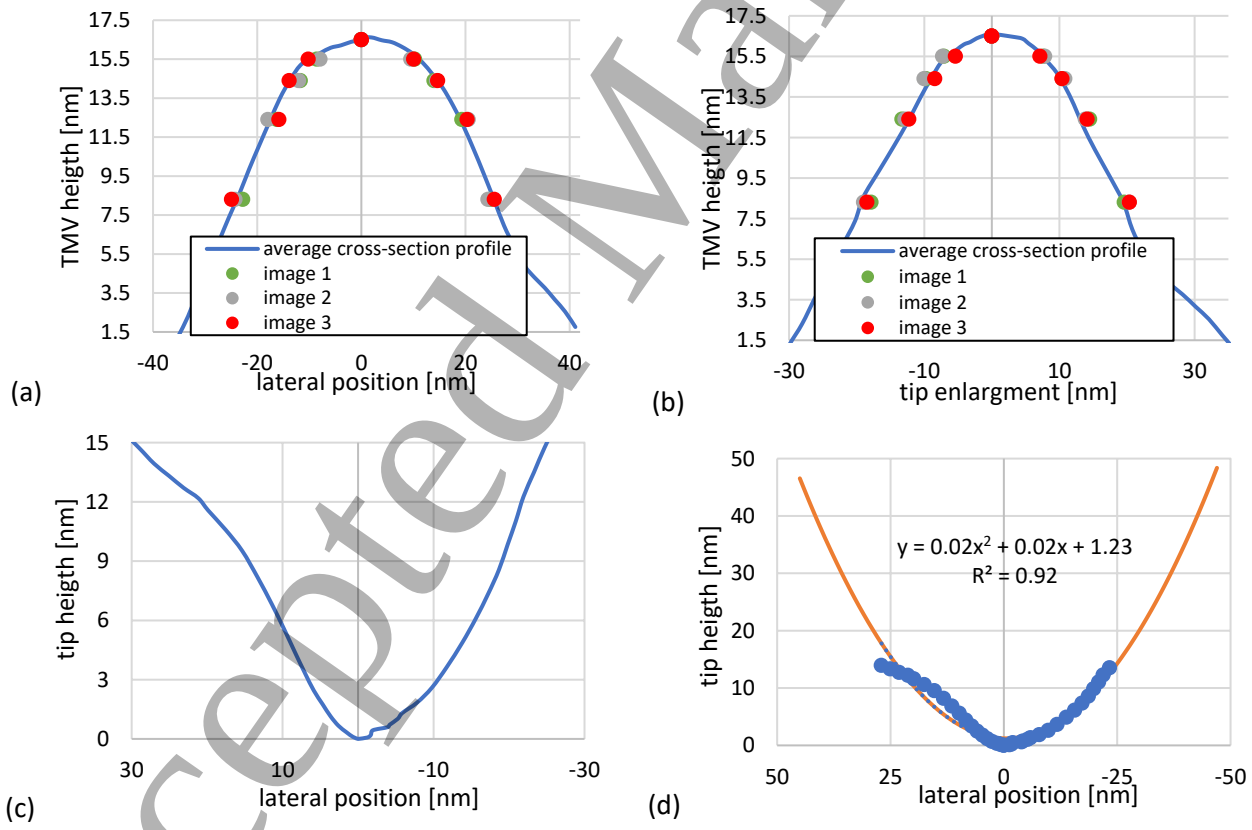

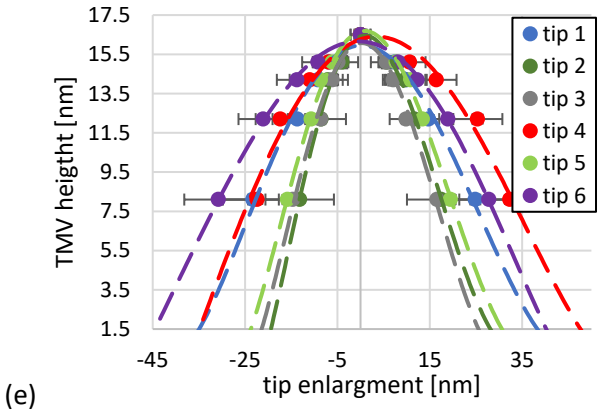

(e)

Figure 9 (a) Average TMV cross-section profile from the analysis of independent images of the same tip. (b) Average tip enlargement profile from the analysis of independent images of the same tip. (c) 2D lateral tip profile from lateral analysis of independent images. (d) Parabolic fit (orange curve) of the tip profile (blue dots). (e) Mean profiles of the enlargement of one tip used for analysing the TMV. The error bars refer to measurements' standard deviation.

Figure 9 (a) and (b) show the comparison between a mean cross-section profile and the profile of the enlargement b for a case study on three subsequent images measured with the same tip.
Figure 9 (c) reports a tip bidimensional profile, that is the negative of the enlargement profile. Figure 9 (d) shows the parabolic fit of the tip profile, thanks to which we can extrapolate the tip shape for heights greater than the highest feature imaged (in this case the TMV step-height).
In Figure 9 (e) are reported the tip enlargements mean values of the 3 samples measured by 6 different tips at heights of about 8 nm, 12 nm, 14 nm, 15 nm and 16.5 nm from the mica substrate.

Note that the bottom 10 % is excluded by all profiles of Figure 9 (a), (b), (c) and (e), because it can contain non-tip artefacts [21].

5. Conclusions

The availability of using well-known 3D nanostructures as tip characterizers is today an issue for critical dimension measurements at the nanoscale by means of AFM instruments. Being one of the main error sources, an accurate correction of the tip shape and size is needed, because AFM images result from the convolution of the probe shape, the sample shape and the tip-sample-substrate interactions. In this work, the Tobacco Mosaic Virus, a stable non-synthetic nanostructure abundantly present in nature, is used as tip geometry characteriser. To do that, TMV virions are characterised in terms of diameter, measured as thickness of the cross-section profile of the cylinder, together with its uncertainty budget. Since the TMV thickness measured is 16.5 nm and it is minor than the nominal value of 18 nm from fibre diffraction measurements, the deformation study due to tip-sample-substrate interactions is performed, using both experimental data and literature models, obtaining a total deformation of about 1.2 nm. Moreover, the elastic modulus of the TMV has been determined using the Hertzian model, giving a value $E_{TMV} = 1.3 \pm 0.6$ GPa. The expanded uncertainty is strongly influenced by the uncertainty of the tip-sample interaction area.

TMV samples are also characterized in terms of lateral dimensions, in order to estimate a 2D tip profile. Using the TMV as the probe, the tip shape is reconstructed by lateral measurements considering the right and left enlargement. The enlargement is calculated by assuming undeformed the circular shape of the

TMV cross-section, and a good repeatability of the reconstructed tip shape is achieved from subsequent imaging of virions. Further studies will be performed to estimate the tip profile at higher heights, by comparison with profiles taken with high-aspect-ratio nanostructures.

Future work will deepen the study of the tip shape reconstruction using TMV as reference materials, since the AFM-based top-height measurements of the virion diameter show a good repeatability with samples kept in normal laboratory conditions. Moreover, a study of the stability along time will be further extended.

Glossary

1D: mono-dimensional
2D: bi-dimensional
3D: three-dimensional
$\alpha_{tip-sam}$: tip-sample elastic deformation
$\alpha_{sam-sub\ MP}$: sample-substrate plastic deformation by MP model (sphere on a plane)
$\alpha_{sam-sub\ JKR}$: sample-substrate plastic deformation by JKR model (sphere on a plane)
$\alpha_{sam-sub\ DMT}$: sample-substrate plastic deformation by DMT model (sphere on a plane)
$\alpha_{sam-sub\ Ch}$: sample-substrate adhesive deformation by Chaudhury *et al.* approach (cylinder on a plane)
$\alpha_{tip-sub}$: tip-substrate elastic deformation
ν: Poisson's ratio
γ: surface energy
a: semi-chord of the circle
b: right/left lateral enlargement
c: half-side contact between the cylinder and the plane
CD: Critical Dimension
CNR – IPSP: Consiglio Nazionale delle Ricerche – Istituto per la Protezione Sostenibile delle Piante
DMT: Derjaguin–Muller–Toporov
h: TMV diameter measured as thickness
D: diameter
E: Young's modulus
E_{red}: reduced elastic modulus
INRiM: Istituto Nazionale di Ricerca Metrologica
JKR: Johnson–Kendall–Roberts
K: equivalent elastic modulus
MP: Maugis–Pollock
Na EDTA: ethylenediaminetetraacetic acid
Na DIECA: sodium diethyldithiocarbamate
NIST: National Institute of Standards and Technology
NMI: National Metrology Institute
mAFM: metrological Atomic Force Microscope
NP: nanoparticle
PTB: Physikalisch–Technische Bundesanstalt
r_{tip}: nominal tip radius
r_{TMV}: TMV radius
s: contact radius between the sphere and the plane
TEM: transmission electron microscopy
TMV: Tobacco Mosaic Virus
P: applied force
w_a: adhesion work
Y: yield point

Acknowledgments

The parent project 15 SIB 09 "3DNano – Traceable three-dimensional nanometrology" is delivered under the EMPIR initiative, which is co-funded by the EU's Horizon 2020 research and innovation programme and the EMPIR Participating States.

The authors wish to thank the internship students Marco Carofiglio, Manuel Damiani, Marco Giordano and Thi Anh Linh Nguyen of "Politecnico di Torino" for their preliminary studies in the tip-sample interaction.

ORCID iDs

Gian Bartolo Picotto https://orcid.org/0000-0002-7014-0629

Marta Vallino http://orcid.org/0000-0003-1465-3574

Luigi Ribotta https://orcid.org/0000-0001-5334-5246

References

[1] F. Meli, T. Klein, E. Buhr, C. Frase, G. Gleber, M. Krumrey, A. Duta, S. Duta, V. Korpelainen, R. Bellotti, G. B. Picotto, R. D. Boyd, A. Cuenat, Traceable size determination of nanoparticles, a comparison among European metrology institutes, *Meas. Sci. Technol.*, 2012, 23, 125005
DOI: 10.1088/0957-0233/23/12/125005
[2] Supplementary Comparison on Nanoparticle Size (APMP.L-S5), https://www.bipm.org/kcdb/comparison?id=1149, web access in November 2019
DOI: 10.1088/0026-1394/56/1A/04004
[3] M. J. Puttock, E. G. Thwaite, Elastic Compression of Spheres and Cylinders at Point and Line Contact, National Standards Laboratory Technical Paper No. 25, 1969, page 18
[4] K. L. Johnson, K. Kendall, A. D. Roberts, Surface energy and the contact of elastic solids, *Proc. R. Soc. Lond. A* 324, 301–313 (1971)
DOI: 10.1098/rspa.1971.0141
[5] B. V. Derjaguin, V. M. Muller, Y. P. Toporov, Effect of contact deformations on the adhesion of particles, *J. Colloid Interf. Sci*. 53, 314–326 (1975)
DOI: 10.1016/0021-9797(75)90018-1
[6] D. Maugis, H. M. Pollock, Surface forces, deformation and adherence at metal microcontacts, 32, 9, 1984, 1323-1334
DOI: 10.1016/0001-6160(84)90078-6
[7] D. Guo, G. Xie, J. Luo, Mechanical properties of nanoparticles: basics and applications, *J. Phys. D: Appl. Phys.* 47 (2014) 013001 (25pp)
DOI: 10.1088/0022-3727/47/1/013001
[8] A. San Paulo, R. Garcia, High-Resolution Imaging of Antibodies by Tapping-Mode Atomic Force Microscopy: Attractive and Repulsive Tip-Sample Interaction Regimes, 78, 3, 1559-1605, 2000
DOI: 10.1016/S0006-3495(00)76712-9
[9] A. D. Slattery, A. J. Blanch, J. S. Quinton, Efficient attachment of carbon nanotubes to conventional and high-frequency AFM probes enhanced by electron beam processes, Nanotechnology 24 (23), 235705
DOI: 10.1088/0957-4484/24/23/235705
[10] N. Sebaihi, B. De Boeck, Y. Yuana, R. Nieuwland, J. Pétry, Dimensional characterization of extracellular vesicles using atomic force microscopy, *Meas. Sci. Technol*., 28 (2017) 034006 (8pp)
DOI: 10.1088/1361-6501/28/3/034006
[11] M. T. Postek, Critical Issues in Scanning Electron Microscope Metrology, *J. Res Natl Inst Stand Technol.* 1994; 99:641
[12] EMPIR 17 NRM 04 nPSize "Improved traceability chain of nanoparticle size measurements" project, https://www.euramet.org/research-innovation/search-research-

projects/details/?eurametCtcp_project_show%5Bproject%5D=1549&eurametCtcp_project%5Bback%5D=1081&cHash=70b686fdd8cde8926b1ce1a5e168f7b4, web access in September 2019
[13] P. M. Williams, K. M. Shakesheff, M. C. Davies, D. E. Jackson, C. J. Roberts (1996) Blind reconstruction of scanning probe image data, *JVST B* 14(2), 1557-62
DOI: 10.1116/1.589138
[14] J. S. Villarrubia, Algorithms for Scanned Probe Microscope Image Simulation, Surface Reconstruction, and Tip Estimation, *J Res Natl Inst Stand Technol.* 1997 Jul-Aug; 102(4): 425–454
DOI: 10.6028/jres.102.030
[15] G. Dahlen, M. Osborn, N. Okulan, W. Foreman, A. Chand, Tip characterization and surface reconstruction of complex structures with critical dimension atomic force microscopy, *Journal of Vacuum Science & Technology B*, 23, 6, 2005
DOI: 10.1116/1.2101601
[16] K. A. Ramirez-Aguilar, K. L. Rowlen, Tip characterization from AFM images of nanometric spherical particles, *Langmuir* 14 (1998) 2562–2566
DOI: 10.1021/la971277o
[17] M. P. Seah, S. J. Spencer, P. J. Cumpson, J. E. Johnstone, Sputter- Induced and filament formation on InP and AFM tip shape determination, *Surf. Interface Anal.,* 29, 782, 2000
[18] F. Tian, X. Qian, J. S. Villarrubia, Blind estimation of general tip shape in AFM imaging, *Ultramicroscopy*, 1, 109, 2008, 44-53
DOI: 10.1016/j.ultramic.2008.08.002
[19] X. Qian, J. S. Villarrubia, General three-dimensional image simulation and surface reconstruction in scanning probe microscopy using a dexel representation, *Ultramicroscopy*, 1, 108, 2007, 29-42
DOI: 10.1016/j.ultramic.2007.02.031
[20] J. Wan, L. Xu, S. Wu, X. Hu, Investigation on Blind Tip Reconstruction Errors Caused by Sample Features, *Sensors* 2014, 14, 23159-23175
DOI: 10.3390/s141223159
[21] N. G. Orji, H. Itoh, C. Wang, R. G. Dixson, P. S. Walecki, S. W. Schmidt, B. Irmer, Tip Characterization Method using Multi-feature Characterizer for CD-AFM, *Ultramicroscopy*, 162, 2016, 25-34
DOI: 10.1016/j.ultramic.2015.12.003
[22] G. R. Bushell, G. S. Watson, S. A. Holt, S. Myhra, Imaging and nano-dissection of tobacco mosaic virus by atomic force microscopy, *Journal of Microscopy.* 180, 2, 1995, 174-181
DOI: 10.1111/j.1365-2818.1995.tb03673.x
[23] Y. F. Drygin, O. A. Bordunova, M. O. Gallyamov, I. V. Yaminsky, Atomic force microscopy examination of tobacco mosaic virus and virion RNA, *FEBS Letters*, 425 (1998) 217-221
DOI: 10.1016/S0014-5793(98)00232-4
[24] A. Eleta-Lopez, A. Calo, Key factors of scanning a plant virus with AFM in air and aqueous solution, *Microscopy Research and Technique*, Wiley Periodicals, 2016
DOI: 10.1002/jemt.22741
[25] J. M. Alonso, M.Ł. Górzny, A. M. Bittner, The physics of tobacco mosaic virus and virus-based devices in biotechnology, *Trends Biotechnol.*, 31, 9, 530-538, 2013
DOI: 10.1016/j.tibtech.2013.05.013
[26] K. Namba, G. Stubbs, Structure of tobacco mosaic virus at 3.6 Å resolution: implications for assembly, Science, 21, 1986
DOI: 10.1126/science.3952490
[27] P. J. G. Butler, Self-assembly of tobacco mosaic virus: the role of an intermediate aggregate in generating both specificity and speed, *Phil.Trans. R. Soc. Lond. B* (1999) 354, 537-550
DOI: 10.1098/rstb.1999.0405
[28] A. Klug, The tobacco mosaic virus particle: structure and assembly, *Phil.Trans. R. Soc. Lond. B*, 1999; 354, 531–535
DOI: 10.1098/rstb.1999.0404
[29] G. Stubbs, Fibre diffraction studies of filamentous viruses, *Rep. Prog. Phys.*, 64, 1389-1425, 2001

DOI: 10.1088/0034-4885/64/11/201
[30] M.-H. Trinh, M. Odorico, L. Bellanger, M. Jacquemond, P. Parot, J.-L. Pellequer, Tobacco mosaic virus as an AFM tip calibrator, *J. Mol. Recognit.* 2011; 24: 503–510
DOI: 10.1002/jmr.1118
[31] http://www.mirri-it.it/index.php/corners/national-research-council-cnr/, web access December 2019
[32] N. G. Orji, H. Itoh, C. Wang, R. G. Dixson, Technique for AFM Tip Characterization*, Proc. of SPIE* Vol. 9173, 917305, 2014
DOI: 10.1117/12.2062759
[33] G. B. Picotto M. Pisani, A sample scanning system with nanometric accuracy for quantitative SPM measurements, *Ultramicroscopy*, 86, 2001, 247-254
[34] ISO 1:2016, Geometrical product specifications (GPS) — Standard reference temperature for the specification of geometrical and dimensional properties, https://www.iso.org/standard/67630.html, web access in December 2019
[35] https://www.spmtips.com/afm-tip-hq-nsc15-al-bs, web access January 2020
[36] Image Metrology SPIP, website (https://www.imagemet.com/products/spip/), web access October 2019
[37] C. Godon, J.-M. Teulon, M. Odorico, C. Basset, M. Meillan, L. Vellutini, S. W. Chen, J-L Pellequer, Conditions to minimize soft single biomolecule deformation when imaging with atomic force microscopy, Journal of Structural Biology, 197, 3, 2017, 322-329
DOI: 10.1016/j.jsb.2016.12.011
[38] Y. Lin, H. Komatsu, J. Ma, P. H. Axelsenb, Z. Fakhraai, Quantitative analysis of amyloid polymorphism using height histograms to correct for tip convolution effects in atomic force microscopy imaging, Royal Society of Chemistry Advances, 2016, 6, 114286
DOI: 10.1039/c6ra24031c
[39] O. V. Sinitsyna, N. O. Kalinina, K. McGeachy, E. Whale, D. Hepworth, A. J. Love, M. E. Taliansky, I. V. Yaminsky, Interaction between nanocellulose and tobacco mosaic viruslike particles: an atomic force microscopy study, Cellulose (2020)
DOI: 10.1007/s10570-020-02978-1
[40] N. Stitz, S. Eiben, P. Atanasova, N. Domingo, A. Leineweber, Z. Burghard, J. Bill, Piezoelectric Templates – New Views on Biomineralization and Biomimetics, Nature Scientific Report, 6, 26518 (2016)
DOI: 10.1038/srep26518
[41] F. A. Schabert, J. P. Rabe, Vertical dimension of hydrated biological samples in tapping mode scanning force microscopy, Biophysical Journal, 70, 3, 1996, 1514-1520
DOI: 10.1016/S0006-3495(96)79713-8
[42] C. A. Clifford, M. P Seah, E. E. Flater, G. Zacharackis-Jutz, B. Dumba, I. White, Determination of AFM probe properties, *European Microscopy Congress*, Manchester, 16th - 21st September 2012
http://www.emc2012.org.uk/documents/Abstracts/Abstracts/EMC2012_1103.pdf, web access November 2019
[43] J. P. Cleveland, S. Manne, D. Bocek, P. K. Hansma, Nondestructive method for determining the spring constant of cantilevers for scanning force microscopy, Review of Scientific Instruments 64, 403 (1993)
DOI: 10.1063/1.1144209
[44] J. E. Sader, I. Larson, P. Mulvaney, Method for the calibration of atomic force microscope cantilevers, Review of Scientific Instruments 66, 3789 (1995)
DOI: 10.1063/1.1145439
[45] J. E. Sader, J. W. M. Chon, P. Mulvaney, Calibration of rectangular atomic force microscope cantilevers, Review of Scientific Instruments 70, 3967 (1999)
DOI: 10.1063/1.1150021
[46] C. A Clifford, M. P Seah, Improved methods and uncertainty analysis in the calibration of the spring constant of an atomic force microscope cantilever using static experimental methods, 2009, Meas. Sci. Technol., 20, 125501
DOI: 10.1088/0957-0233/20/12/125501

[47] A. D. Slattery, A. J. Blanch, J. S. Quinton, C. T. Gibson, Calibration of atomic force microscope cantilevers using standard and inverted static methods assisted by FIB-milled spatial markers, 2013 Nanotechnology 24 015710
DOI: 10.1088/0957-4484/24/1/015710
[48] C. T. Gibson, D. A. Smith, C. J. Roberts, Calibration of silicon atomic force microscope cantilevers, 2005 Nanotechnology 16 234
DOI: 10.1088/0957-4484/16/2/009
[49] A. D. Slattery, J. S Quinton, C. T. Gibson, Atomic force microscope cantilever calibration using a focused ion beam, Nanotechnology, 23, 28, 2012
DOI: 10.1088/0957-4484/23/28/285704
[50] https://sadermethod.org/, web access January 2020
[51] J. E. Sader, R. Borgani, C. T. Gibson, D. B. Haviland, M. J. Higgins, J. I. Kilpatrick, J. Lu, P. Mulvaney, C. J. Shearer, A. D. Slattery, P. Thoren, J. Tran, H. Zhang, H. Zhang, T. Zheng, A virtual instrument to standardise the calibration of atomic force microscope cantilevers, Review of Scientific Instruments, 87 093711 (2016)
DOI: 10.1063/1.4962866
[52] M. R. Falvo, S. Washburn, R. Superfine, M. Finch, F. P. Brooks Jr., V. Chi, R. M. Taylor II, Manipulation of Individual Viruses: Friction and Mechanical Properties, *Biophysical Journal*, 72, 1396-1403, 1996
DOI: 10.1016/S0006-3495(97)78786-1
[53] O. I. Kiselyova, M. O. Gallyamov, N. S. Nasikan, I. V. Yaminsky, O. V. Karpova, V. K. Novikov, Scanning Probe Microscopy of Biomacromolecules: Nucleic Acids, Proteins And Their Complexes, in Frontiers of Multifunctional Nanosystems by E. Buzaneva, P. Scharff, Frontiers of Multifunctional Nanosystems, NATO Science Series (Series II: Mathematics, Physics and Chemistry), 57, 321-330, 2002
DOI: 10.1007/978-94-010-0341-4_24
[54] A. Schmatulla, N. Maghelli, O. Marti, Micromechanical properties of tobacco mosaic viruses, Journal of Microscopy, 225, 3, 2007, 264–268
DOI: 10.1111/j.1365-2818.2007.01741.x
[55] Y. Zhao, Z. Ge, J. Fang, Elastic modulus of viral nanotubes, *Physical Review E*, 78, 031914, 2008
DOI: 10.1103/PhysRevE.78.031914
[56] H. Wang, X. Wang, T. Li, B. Lee, Nanomechanical characterization of rod-like superlattice assembled from tobacco mosaic viruses, Journal of Applied Physics, 113, 024308 (2013)
DOI: 10.1063/1.4774103
[57] S. P. Baker, Nanoindentation Techniques, Encyclopedia of Materials: Science and Technology (Second Edition), 2001
DOI: 10.1016/B0-08-043152-6/01030-5
[58] M. A. Hopcroft, W. D. Nix, T, W. Kenny, What is the Young's Modulus of Silicon?, Journal of Microelectromechanical Systems, 19, 2, 229-238, 2010
DOI: 10.1109/JMEMS.2009.2039697
[59] Mechanical properties of silicon, https://www.el-cat.com/silicon-properties.htm, web access July 2019
[60] I. Misumi, K. Sugawara, K. Takahata, K. Takahashi, K. Ehara, Size measurements of standard nanoparticles using metrological atomic force microscope and evaluation of their uncertainties, *Precision Engineering*, 51, 2018, 691-701
DOI: 10.1016/j.precisioneng.2017.11.013
[61] X. D. Wang, B. Chen, H. F. Wang, Z. S. Wang, Adhesion between submicrometer polystyrene spheres, Powder Technol, 214 (2011), pp. 447-450
DOI: 10.1016/j.powtec.2011.08.047
[62] M. K. Chaudhury, T. Weaver, C. Y. Hui, E. J. Kramer, Adhesive contact of cylindrical lens and a flat sheet, J. Appl. Phys. 80 (1), 1996
DOI: 10.1063/1.362819
[63] A. Castellanos-Gomez, M. Poot, A. Amor-Amorós, G. A. Steele, H. S. J. van der Zant, N. Agraït, G. Gabino Rubio-Bollinger, Mechanical properties of freely suspended atomically thin dielectric layers of mica, *Nano Research*, 5, 8 (2012), 550-557

DOI: 10.1007/s12274-012-0240-3
[64] E. N. Vasina, E. Paszek, D. V. Nicolau, Jr., D. V. Nicolau, The BAD project: data mining, database and prediction of protein adsorption on surfaces, *Lab Chip*, 2009, 9, Supplementary Information
DOI: 10.1039/B813475H
[65] A. Nicolet, F. Meli, Spherical polystyrene particle deformation measured with the AFM, *Meas. Sci. Technol.* 28 (2017) 034003
DOI: 10.1088/1361-6501/28/3/034003
[66] G. Dai, K. Hahm, H. Bosse, R. G. Dixson, Comparison of line width calibration using critical dimension atomic force microscopes between PTB and NIST, *Meas. Sci. Technol.,* 2017, 28, 065010
DOI: 10.1088/1361-6501/aa665b